Fuzzy steering control for autonomous vehicles under actuator saturation: Design and experiments

Tran Anh-Tu Nguyen, Chouki Sentouh, Jean-Christophe Popieul

Fuzzy Steering Control for Autonomous Vehicles under Actuator Saturation: Design and Experiments

Article *in* Journal of the Franklin Institute · December 2018

DOI: 10.1016/j.jfranklin.2017.11.027

3 authors, including:

Anh-Tu Nguyen
Université Polytechnique Hauts-de-France
140 PUBLICATIONS **2,084** CITATIONS
SEE PROFILE

Chouki Sentouh
LAMIH UMR CNRS 8201 Hauts-de-France Polytechnic University
114 PUBLICATIONS **2,057** CITATIONS
SEE PROFILE

Fuzzy Steering Control for Autonomous Vehicles under Actuator Saturation: Design and Experiments

Anh-Tu Nguyen*, Chouki Sentouh, Jean-Christophe Popieul

Laboratory LAMIH UMR CNRS 8201, University of Valenciennes, France

Abstract

This paper presents a new control method for autonomous vehicles. The design goal is to perform the automatic lane keeping under multiple system constraints, namely actuator saturation of the steering system, roads with unknown curvature and uncertain lateral wind force. Such system constraints are *explicitly* taken into account in the control design procedure. To achieve this goal, we propose a new constrained Takagi-Sugeno fuzzy model-based control method using fuzzy Lyapunov control framework. The resulting non-parallel distributed compensation controller is able to handle not only various system constraints but also a large variation range of vehicle speed. In particular, Taylor's approximation method is exploited to reduce not only the numerical complexity for real-time implementation but also the conservatism of the results. The design conditions are strictly expressed in terms of linear matrix inequalities which can be efficiently solved with available numerical solvers. The effectiveness of the proposed control method is demonstrated through both simulation and hardware experiments with various driving scenarios.

Keywords: Autonomous vehicles, lane keeping control, Takagi-Sugeno fuzzy systems, actuator saturation, fuzzy Lyapunov functions, linear matrix inequality.

1. Introduction

Nowadays, automobiles have become essential in our society since they provide individuals a great freedom for traveling. At the same time, road accident still remains one of the main mortality causes of our daily life despite huge prevention efforts from governments and automotive industry. As a consequence, the field

*Corresponding author.
Email address: nguyen.trananhtu@gmail.com (Anh-Tu Nguyen)

To be published in the Journal of The Franklin Institute

of intelligent vehicles, including the issue of autonomous vehicles, has attracted a growing attention from both academic and industrial settings with the aim of improving safety, comfort, and efficiency [1–5]. Intelligent vehicles make use of sensing and intelligent algorithms to understand the vehicle's immediate environment, for either assisting the driver or fully controlling the vehicle [6–9]. In this context, our research is concerned with the automatic control of the steering system (also known as lateral control) for autonomous vehicles.

Up to now, several lateral controllers have been developed for the lane keeping control problem in the literature [3, 4, 7, 10, 11]. The authors in [12] have presented an automatic-steering control architecture based on a combination of fuzzy logic and PID control. In that work, the driver actions have been considered as a system disturbance which is systematically rejected by the control system. A switching control scheme based on Lyapunov stability theorem and LMI (linear matrix inequality) optimization has been proposed in [10] to avoid lane departures when the driver has a lapse of attention. In [13], an automatic lane-keeping control is combined with driver's steering for obstacle avoidance and lane-change maneuvers without using switching strategies between these both control actions. A nested PID steering control strategy has been proposed and experimentally validated for an autonomous vehicle in [14] in the case of roads with unknown curvature. A real-vehicle application being able to manage autonomous-steering and perform human-like tracking has been also developed in [15]. Robust dynamic output feedback controllers based on a driver-vehicle model have been proposed in [8, 9] to assist the driver for tracking the reference trajectory. Note that in most of the available works, the longitudinal speed has been considered as a *constant* to ease the control design. Moreover, existing works have not *explicitly* taken into account the saturation effects of the steering system in the control design procedure. This can lead to serious degradation of control performance, in many cases, the stability may be lost [16–18].

In recent years, stability analysis and control design based on Takagi-Sugeno (T-S) fuzzy models [19] have become the most popular research platform in fuzzy model-based control [16, 20–23]. This fact is due to many outstanding features of T-S fuzzy models for control purposes [20]. First, they can be used as a universal approximator for any smooth nonlinear system. In particular, the sector nonlinearity approach provides an exact T-S representation of a given nonlinear model in a compact set. Second, thanks to their polytopic structure with linear systems in the consequent parts, T-S fuzzy models allow to extend some linear control concepts to nonlinear systems. Moreover, T-S fuzzy-model-based control techniques have been successfully applied to various engineering applications [7, 22, 24, 25]. In T-S fuzzy control framework, a norm-bounded approach has been used in [24] to handle the control input limitations. The resulting low-gain non-saturated con-

trollers are generally conservative and offer poor control performance [17, 26]. Polytopic representation of the saturation nonlinearity has been employed in [26–28]. Based on the technique of extended non-quadratic boundedness, the authors in [18] have proposed non-parallel distributed compensation controllers for T-S fuzzy systems subject to input and state constraints and bounded noise. An equivalent augmentation form of the closed-loop system has been exploited together with a generalized saturation sector condition in [29] for the control design of a class of input-constrained Takagi-Sugeno fuzzy systems. In [30], the control input limitations have been taken into account in the design procedure using an LP (linear programming) approach.

Motivated by the above control issues, this paper aims at developing a new robust control method for automatic lane keeping of autonomous vehicles subject to multiple system constraints, i.e. actuator saturation, roads with unknown curvature and uncertain lateral wind force. The contributions are summarized as follows.

- Using T-S fuzzy modeling to represent the vehicle dynamics, the proposed automatic lane keeping method can handle a large variation range of vehicle speed. Moreover, Taylor's approximation method is used to reduce significantly the numerical complexity of the vehicle T-S fuzzy model. This eases the real-time control implementation and also reduces the design conservatism.

- The actuator saturation of the steering system is *explicitly* taken into account in the control design via a generalized sector condition. In particular, a fuzzy Lyapunov function is used for theoretical developments to reduce further the conservatism. The design conditions are expressed in terms of LMIs which can be easily solved with numerical solvers.

- The practical performance of the proposed lane keeping control method is successfully validated through both simulations and hardware experiments.

The paper is organized as follows. Section 2 presents the key elements of vehicle modeling. The transformation from a continuous vehicle model to its corresponding discrete version via Euler's approximation is also given. In Section 3, we first formulate the control problem, then the design conditions are derived in fuzzy Lyapunov control framework. Section 4 highlights the application of the proposed method to the studied autonomous vehicle. Both simulation and hardware experiments to demonstrate the lane keeping performance are presented in Section 5. Finally, concluding remarks are reported in Section 6.

Notation. For an integer number r, Ω_r denotes the set $\{1, 2, \ldots, r\}$. I denotes the identity matrix of appropriate dimension. For a square matrix X, $X > 0$ means that X is positive definite. The ith element of a vector u is denoted $u_{(i)}$ and $X_{(i)}$

denotes the ith row of matrix X. The symbol $\star$ stands for matrix blocks that can be deduced by symmetry. For a positive definite function $\mathbb{V}(x)$ defined on $\mathbb{R}^{n_x}$, we denote $\mathcal{E}_{\mathbb{V}} = \{x \in \mathbb{R}^{n_x} : \mathbb{V}(x) \leq 1\}$. The scalar functions $\eta_1, \ldots, \eta_r$ are said to verify the convex sum property if

$$\eta_i \geq 0, \quad \sum_{i=1}^{r} \eta_i = 1 \tag{1}$$

For such scalar functions with any argument θ, we denote

$$Y_\theta = \sum_{i=1}^{r} \eta_i(\theta) Y_i, \quad Y_\theta^{-1} = \left(\sum_{i=1}^{r} \eta_i(\theta) Y_i \right)^{-1} \tag{2}$$

where the matrices Y_i are of appropriate dimensions. Throughout this paper, the time argument will be dropped when convenient.

2. Vehicle Modeling

This section details the modeling of the studied autonomous vehicle.

2.1. Road-Vehicle Model

In order to investigate the vehicle motions and to evaluate the control performance, the vehicle handling dynamics in the horizontal plane are represented by the non-linear single track vehicle model [2, 14], see Figure 1. Then, the vehicle dynamics is given by

$$\begin{aligned} M\left(\dot{v}_x - r v_y\right) &= F_{xf}\cos\delta - F_{yf}\sin\delta + F_{xr} \\ M\left(\dot{v}_y + r v_x\right) &= F_{xf}\sin\delta + F_{yf}\cos\delta + F_{yr} + f_w \\ I_z \dot{r} &= l_f\left(F_{xf}\sin\delta + F_{yf}\cos\delta\right) - l_r F_{yr} + l_w f_w \end{aligned} \tag{3}$$

For brevity, the vehicle nomenclature used in this work are given in Table 1. The front and rear longitudinal forces F_{xi} with $i = f, r$ and the front and rear lateral forces F_{yi} with $i = f, r$ are modeled according to the Pacejka's tire model [31] (known also as *magic* formula):

$$F_{ki}\left(\alpha_i\right) = D_i \sin\left\{C_i \arctan\left[(1 - E_i)B_i\alpha_i + E_i \arctan\left(B_i\alpha_i\right)\right]\right\} \tag{4}$$

where $k = x, y$ and $i = f, r$. The Pacejka parameters B_i, C_i, D_i and E_i in (4) depend on the characteristics of the tyre, road and the vehicle operating conditions.

For lateral control purposes, the nonlinear vehicle model (3) will be simplified. To this end, we consider normal driving situations and *small* angle approximation

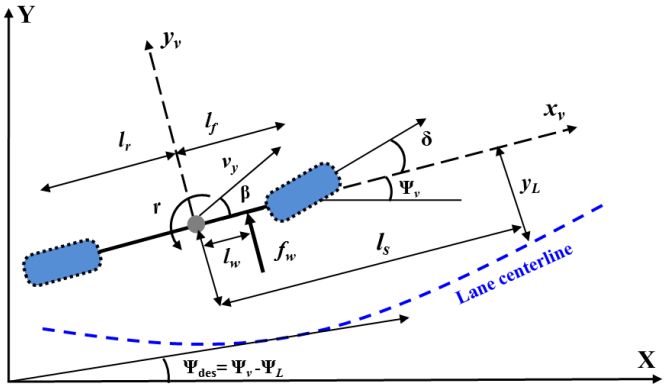

Figure 1: Single track vehicle model.

[2]. As a result, the lateral speed and the lateral tire forces can be computed with the following expressions:

$$\begin{aligned} v_y &= v_x\beta \\ F_{yf} &= 2C_f\alpha_f = 2C_f\left(\frac{v_y + l_f r}{v_x} - \delta\right) \\ F_{yr} &= 2C_r\alpha_r = 2C_r\frac{v_y - l_r r}{v_x} \end{aligned} \tag{5}$$

where C_f and C_r are respectively the front and rear cornering stiffness coefficients. This work focuses on the lateral motion of the vehicle. Then, the longitudinal dynamics is decoupled from the lateral dynamics and the longitudinal speed is considered as a time-varying parameter for control purposes. Combining this fact with (3)-(5), the vehicle lateral dynamics is given by

$$\begin{bmatrix}\dot{\beta}\\ \dot{r}\end{bmatrix} = \begin{bmatrix}a_{11} & a_{12}\\ a_{21} & a_{22}\end{bmatrix}\begin{bmatrix}\beta\\ r\end{bmatrix} + \begin{bmatrix}b_1\\ b_2\end{bmatrix}\delta + \begin{bmatrix}e_1\\ e_2\end{bmatrix} f_w \tag{6}$$

where the matrix elements in (6) are defined as follows:

$$a_{11} = -\frac{2(C_r + C_f)}{Mv_x}, \quad a_{12} = \frac{2(l_r C_r - l_f C_f)}{Mv_x^2} - 1, \quad b_1 = \frac{2C_f}{Mv_x}, \quad e_1 = \frac{1}{Mv_x}$$
$$a_{21} = \frac{2(l_r C_r - l_f C_f)}{I_z}, \quad a_{22} = \frac{-2(l_r^2 C_r + l_f^2 C_f)}{I_z v_x}, \quad b_2 = \frac{2l_f C_f}{I_z}, \quad e_2 = \frac{l_w}{I_z}.$$

Table 1: Vehicle model parameters

Symbol	Description
$v_{x,y}$	longitudinal/lateral speed
β	sideslip angle at the center of gravity (CG)
r	vehicle yaw rate
f_w	lateral wind force
ρ_r	road curvature
δ	steering angle
M	total mass of the vehicle
l_f	distance from CG to the front axle
l_r	distance from CG to the rear axle
l_w	distance from CG to the impact center of the wind force
l_s	look-ahead distance
η_t	tire length contact
I_z	vehicle yaw moment of inertia
C_f	front cornering stiffness
C_r	rear cornering stiffness

2.2. Road-Vehicle Positioning

The lane-keeping dynamics can be represented via two supplementary measurements provided by the vision system [2], namely the lateral deviation error y_L from the centerline of the lane projected forward a lookahead distance l_s, and the heading error ψ_L between the tangent to the road and the vehicle orientation, see Figure 1. Then, the dynamics representing the vehicle positioning on the road is given by

$$\begin{cases} \dot{y}_L = v_x\beta + l_s r + v_x\psi_L \\ \dot{\psi}_L = r - v_x\rho_r \end{cases} \tag{7}$$

where ρ_r denotes the unknown road curvature.

2.3. Vehicle Control-Based Model

From the bicycle vehicle model (6), the dynamics for lane tracking (7), the road-vehicle model used for control purposes can be expressed as follows:

$$\dot{x}(t) = A_v x(t) + B_{vu}u(t) + B_{vw}w(t) \tag{8}$$

where $x = \begin{bmatrix}\beta & r & \psi_L & y_L\end{bmatrix}^\top$ is the vehicle state vector, $w = \begin{bmatrix}f_w & \rho_r\end{bmatrix}^\top$ is the disturbance vector, and the control input is the steering angle $u = \delta$. The system

matrices of the control-based model (8) are given by

$$A_v = \begin{bmatrix} a_{11} & a_{12} & 0 & 0 \\ a_{21} & a_{22} & 0 & 0 \\ 0 & 1 & 0 & 0 \\ v_x & l_s & v_x & 0 \end{bmatrix}, \; B_{vu} = \begin{bmatrix} b_1 \\ b_2 \\ 0 \\ 0 \end{bmatrix}, \; B_{vw} = \begin{bmatrix} e_1 & 0 \\ e_2 & 0 \\ 0 & -v_x \\ 0 & 0 \end{bmatrix}.$$

For simulation and experiment studies, the following system parameters are considered in this paper:

$$\begin{aligned} &M = 2025 \text{ [kg]}, && l_f = 1.3 \text{ [m]}, && l_r = 1.6 \text{ [m]}, \\ &l_w = 0.4 \text{ [m]}, && l_s = 5 \text{ [m]}, && \eta_t = 0.13 \text{ [m]}, \\ &I_z = 2800 \text{ [kgm}^2\text{]}, && C_f = 57000 \text{ [N/rad]}, && C_r = 59000 \text{ [N/rad]}. \end{aligned}$$

To ease the real-time implementation on the vehicle Electronic Control Unit (ECU), the numerical state-feedback controller is directly synthesized in the discrete-time domain. To this end, the well-known Euler's approximation

$$\dot{x}(t) \approx \frac{x(\kappa+1) - x(\kappa)}{T_e}$$

is used to obtain the following discrete-time version of the continuous-time vehicle system (8):

$$\boldsymbol{\Sigma}_v(v_x): \quad x(\kappa+1) = \mathbf{A}x(\kappa) + \mathbf{B}_u u(\kappa) + \mathbf{B}_w w(\kappa) \tag{9}$$

where $z(\kappa)$ denotes the value of the signal z taken at the $\kappa-$instant, $T_e = 0.01s$ is the sampling time of the ECU, and the system matrices are given by

$$\mathbf{A} = I + T_e A_v, \quad \mathbf{B}_u = T_e B_{vu}, \quad \mathbf{B}_w = T_e B_{vw} \tag{10}$$

The discrete-time vehicle system $\boldsymbol{\Sigma}_v$ in (9) is exploited later for control purposes.

3. Control Design for Input-Saturated Takagi-Sugeno Fuzzy Systems

This section presents the theoretical development of a new control method for disturbed T-S fuzzy systems subject to actuator saturation. The design conservatism of the proposed method compared to existing literature is also studied.

3.1. Problem Definition

Consider the discrete-time T-S fuzzy system subject to control input saturation of the following form:

$$\begin{cases} x(\kappa+1) = \sum_{i=1}^{r} \eta_i(\theta) \left(A_i x(\kappa) + B_i^u \operatorname{sat}(u(\kappa)) + B_i^w w(\kappa) \right) \\ z(\kappa) = \sum_{i=1}^{r} \eta_i(\theta) C_i x(\kappa) \end{cases} \tag{11}$$

where $x \in \mathbb{R}^{n_x}$ is the system state, $u \in \mathbb{R}^{n_u}$ is the control input, $w \in \mathbb{R}^{n_w}$ is the disturbance, $z \in \mathbb{R}^{n_z}$ is the performance output, and $\theta \in \mathbb{R}^p$ is the vector of premise variables. The constant matrices A_i, B_i^u, B_i^w, C_i, $i \in \Omega_r$, are of appropriate dimensions and r is the number of model rules. It is worth noting that the normalized membership functions $\eta_i(\theta)$, $i \in \Omega_r$, satisfy the convex sum property defined in (1). The standard input saturation is defined by

$$\operatorname{sat}(u_{(l)}) = \operatorname{sign}(u_{(l)}) \min \left(\left| u_{(l)} \right|, u_{\max(l)} \right), \quad l \in \Omega_{n_u}$$

where the control bounds $u_{\max(l)} > 0$ are given. The disturbance signal w in (11) is bounded in amplitude, i.e. it belongs to the following class of function:

$$\mathcal{W}_\phi^\infty = \left\{ w : \mathbb{R}^+ \to \mathbb{R}^{n_w}, \quad w(\kappa)^\top w(\kappa) \leq \phi, \ \kappa \geq 0 \right\}$$

for some $\phi > 0$.

For the control design of the T-S fuzzy system (11), let us consider the non-parallel distributed compensation (non-PDC) control law of the form

$$u(\kappa) = \left(\sum_{i=1}^{r} \eta_i(\theta) G_i \right) \left(\sum_{i=1}^{r} \eta_i(\theta) H_i \right)^{-1} x(\kappa) \tag{12}$$

where H_i, $i \in \Omega_r$, are *nonsingular* matrices. Using the notations defined in (2), the closed-loop system can be rewritten from (11) and (12) as follows:

$$\begin{cases} x(\kappa+1) = \left(A_\theta + B_\theta^u G_\theta H_\theta^{-1} \right) x(\kappa) - B_\theta^u \Psi(u(\kappa)) + B_\theta^w w(\kappa) \\ z(\kappa) = C_\theta x(\kappa) \end{cases} \tag{13}$$

where $\Psi(u) = u - \operatorname{sat}(u)$.

The control goal is to propose a constructive LMI-based method to design a non-PDC controller of the form (12) such that the closed-loop system (13) satisfies the following properties.

Property 1 (*Local internal stability*)**.** There exists a positive definite function $\mathbb{V}(x(\kappa)) = x(\kappa)^\top \sum_{i=1}^{n} \eta_i(\theta) P_i x(\kappa)$ and its associate set $\mathcal{E}_\mathbb{V}$ such that all closed-loop trajectories starting from $\mathcal{E}_\mathbb{V}$ converge exponentially to the origin in the absence of disturbances, i.e. $w = 0$.

Property 2 (*Input-to-state stability and disturbance attenuation*)**.** If $w \neq 0$ and $w \in \mathcal{W}_\phi^\infty$ for some $\phi > 0$, then all closed-loop trajectories of (13) initialized inside $\mathcal{E}_\mathbb{V}$ will be confined in this set. Moreover, there exists a positive scalar γ such that the $\mathcal{L}_\infty-$norm of the performance output signal z is bounded by

$$\|z(\kappa)\|_\infty^2 \leq \gamma,\ x(0) = 0,\ \forall \kappa \geq 0.$$

3.2. Preliminaries

In the sequel, some useful preliminaries for the control design are presented.

Fact 1. Given positive definite matrix $\mathbf{\Phi}$, the following matrix inequality holds for any matrix $\mathbf{M}$ of appropriate dimension:

$$\mathbf{M}^\top \mathbf{\Phi} \mathbf{M} \geq \mathbf{M} + \mathbf{M}^\top - \mathbf{\Phi}^{-1} \tag{14}$$

Proof. Since $\mathbf{\Phi} > 0$, it is clear that

$$(\mathbf{M} - \mathbf{\Phi}^{-1})^\top \mathbf{\Phi} (\mathbf{M} - \mathbf{\Phi}^{-1}) \geq 0 \tag{15}$$

for any matrix $\mathbf{M}$ of appropriate dimension. Then, the inequality (14) follows directly by developing (15).

□

Lemma 1. Consider matrices $G_i \in \mathbb{R}^{n_u \times n_x}$, $H_i \in \mathbb{R}^{n_x \times n_x}$ and $W_i \in \mathbb{R}^{n_u \times n_x}$, for $i \in \Omega_r$, we define the following set:

$$\mathcal{P}_u = \left\{ x \in \mathbb{R}^{n_x} :\ \left| \left(G_\theta H_\theta^{-1} - W_\theta H_\theta^{-1} \right)_{(l)} x \right| \leq u_{\max(l)},\quad l \in \Omega_{n_u} \right\} \tag{16}$$

If $x \in \mathcal{P}_u$, then the following inequality on the dead-zone nonlinearity $\Psi(u)$, where u is defined in (12):

$$\Psi(u)^\top S_\theta^{-1} \left[\Psi(u) - W_\theta H_\theta^{-1} x \right] \leq 0 \tag{17}$$

holds for any positive diagonal matrices $S_i \in \mathbb{R}^{n_u \times n_u}$, and for any scalar functions $\eta_i(\theta)$, $i \in \Omega_r$, satisfying the convex sum property.

Proof. If $x \in \mathcal{P}_u$, then it follows that

$$-u_{\max(l)} \leq (G_\theta H_\theta^{-1} - W_\theta H_\theta^{-1})_{(l)} x \leq u_{\max(l)}, \quad l \in \Omega_{n_u} \tag{18}$$

In order to prove Lemma 1, we have to show that

$$\Psi(u_{(l)})^\top \left(\sum_{i=1}^{r} \eta_i S_{i(l,l)} \right)^{-1} \left[\Psi(u) - \left(W_\theta H_\theta^{-1} \right) x \right]_{(l)} \leq 0, \quad l \in \Omega_{n_u} \tag{19}$$

where $S_{i(l,l)}$, $i \in \Omega_r$, $l \in \Omega_{n_u}$, denotes the diagonal element at the lth row and lth column of the matrix S_i. To this end, three possible cases are distinguished according to the value of $u_{(l)}$.

- **Case 1**: If $-u_{\max(l)} \leq u_{(l)} \leq u_{\max(l)}$, it follows that $\Psi(u_{(l)}) = 0$. Therefore, the relation (17) holds trivially.

- **Case 2**: If $u_{(l)} > u_{\max(l)}$, then

$$\Psi(u_{(l)}) = u_{(l)} - u_{\max(l)} = \left(G_\theta H_\theta^{-1} \right)_{(l)} x - u_{\max(l)} > 0 \tag{20}$$

It follows from (18) that $\left(G_\theta H_\theta^{-1} - W_\theta H_\theta^{-1} \right)_{(l)} x \leq u_{\max(l)}$. Hence

$$\Psi(u_{(l)}) - \left(W_\theta H_\theta^{-1} \right)_{(l)} x = \left(G_\theta H_\theta^{-1} - W_\theta H_\theta^{-1} \right)_{(l)} x - u_{\max(l)} \leq 0 \tag{21}$$

Since $\Psi(u_{(l)}) > 0$ in this case, then the inequality (19) holds.

- **Case 3**: If $u_{(l)} < -u_{\max(l)}$, then

$$\Psi(u_{(l)}) = u_{(l)} + u_{\max(l)} = \left(G_\theta H_\theta^{-1} \right)_{(l)} x + u_{\max(l)} < 0 \tag{22}$$

From (18), we have that $\left(G_\theta H_\theta^{-1} - W_\theta H_\theta^{-1} \right)_{(l)} x \geq -u_{\max(l)}$. Hence

$$\Psi(u_{(l)}) - \left(W_\theta H_\theta^{-1} \right)_{(l)} x = \left(G_\theta H_\theta^{-1} - W_\theta H_\theta^{-1} \right)_{(l)} x + u_{\max(l)} \geq 0 \tag{23}$$

Combining the fact that $\Psi(u_{(l)}) < 0$ in this case with the inequality (23), it follows that (19) holds.

From the above three cases, the proof of Lemma 1 can be concluded. □

Lemma 2. Let Υ_{ij}^k, $i, j, k \in \Omega_r$, be symmetric matrices of appropriate dimensions and $\{\nu_k\}_{k \in \Omega_r}$, $\{\omega_i\}_{i \in \Omega_r}$, be any family of scalar functions satisfying the property of convex sum. The condition $\sum_{k=1}^{r} \sum_{i=1}^{r} \sum_{j=1}^{r} \nu_k \omega_i \omega_j \Upsilon_{ij}^k < 0$ holds if

$$\begin{cases} \Upsilon_{ii}^k < 0, \quad i, k \in \Omega_r \\ \dfrac{2}{r-1} \Upsilon_{ii}^k + \Upsilon_{ij}^k + \Upsilon_{ji}^k < 0, \quad i, j, k \in \Omega_r, \text{ and } i \neq j \end{cases} \tag{24}$$

Lemma 2 is directly extended from the relaxation result in [32, Theorem 2.2]. Other more efficient relaxation techniques can be found in [23] at the expense of high computational costs due to additional slack variables.

3.3. LMI-based Controller Computation for Constrained T-S Fuzzy Systems

The following theorem provides conditions to design a non-PDC controller (12) for the input-saturated T-S system (11).

Theorem 1. Given the T-S fuzzy system (11) where $w \in \mathcal{W}_\phi^\infty$ for some $\phi > 0$ and a positive scalar $\tau_1 < 1$. If there exist positive definite matrices $X_i \in \mathbb{R}^{n_x \times n_x}$, positive diagonal matrices $S_i \in \mathbb{R}^{n_u \times n_u}$, matrices $H_i \in \mathbb{R}^{n_x \times n_x}$, $G_i \in \mathbb{R}^{n_u \times n_x}$, $W_i \in \mathbb{R}^{n_u \times n_x}$ and positive scalars γ, τ_2 such that

$$\begin{bmatrix} H_i + H_i^\top - X_i & \star \\ G_{i(l)} - W_{i(l)} & u_{\max(l)}^2 \end{bmatrix} > 0, \quad i \in \Omega_r,\ l \in \Omega_{n_u} \tag{25}$$

$$\tau_1 - \tau_2 \phi > 0 \tag{26}$$

$$\begin{bmatrix} H_i + H_i^\top - X_i & \star \\ C_j H_i & \gamma I \end{bmatrix} \geq 0, \quad i, j \in \Omega_r \tag{27}$$

$$\Phi_{ii}^k < 0, \quad i, k \in \Omega_r \tag{28}$$

$$\frac{2}{r-1}\Phi_{ii}^k + \Phi_{ij}^k + \Phi_{ji}^k < 0, \quad i, j, k \in \Omega_r, \text{ and } i \neq j \tag{29}$$

where

$$\Phi_{ij}^k = \begin{bmatrix} (\tau_1 - 1)(H_i + H_i^\top - X_i) & \star & \star & \star \\ W_i & -2S_i & \star & \star \\ 0 & 0 & -\tau_2 I & \star \\ A_j H_i + B_j^u G_i & -B_j^u S_i & B_j^w & -X_k \end{bmatrix} \tag{30}$$

Then, the non-PDC controller (12) solves the control problem in Section 3.1.

Proof. Note that if (25) is verified, then it follows that $H_\theta + H_\theta^\top - X_\theta > 0$. Then, the weighting matrix H_θ is *nonsingular* since $X_\theta > 0$. This guarantees the existence of the inverse matrix H_θ^{-1}.

By the relaxation result in Lemma 2 with

$$\nu_k = \eta_k(\theta(\kappa + 1)), \ \ \omega_i = \eta_i(\theta(\kappa)), \quad i, k \in \Omega_r,$$

we can deduce from (28)-(29) with Φ_{ij}^k defined in (30) that

$$\begin{bmatrix} (\tau_1 - 1)(H_\theta + H_\theta^\top - X_\theta) & \star & \star & \star \\ W_\theta & -2S_\theta & \star & \star \\ 0 & 0 & -\tau_2 I & \star \\ A_\theta H_\theta + B_\theta^u G_\theta & -B_\theta^u S_\theta & B_\theta^w & -X_{\theta+} \end{bmatrix} < 0 \tag{31}$$

Using the matrix property (14) of Fact 1 with $\mathbf{M} = H_\theta$ and $\mathbf{\Phi} = X_\theta^{-1} = P_\theta$, the inequality (31) implies clearly that

$$\begin{bmatrix} (\tau_1 - 1)H_\theta^\top P_\theta H_\theta & \star & \star & \star \\ W_\theta & -2S_\theta & \star & \star \\ 0 & 0 & -\tau_2 I & \star \\ A_\theta H_\theta + B_\theta^u G_\theta & -B_\theta^u S_\theta & B_\theta^w & -X_{\theta+} \end{bmatrix} < 0 \tag{32}$$

Pre- and post-multiplying (32) with $\operatorname{diag}\left(H_\theta^{-1}, S_\theta^{-1}, I, I\right)$ yields

$$\begin{bmatrix} (\tau_1 - 1)P_\theta & \star & \star & \star \\ S_\theta^{-1} W_\theta H_\theta^{-1} & -2S_\theta^{-1} & \star & \star \\ 0 & 0 & -\tau_2 I & \star \\ A_\theta + B_\theta^u G_\theta H_\theta^{-1} & -B_\theta^u & B_\theta^w & -X_{\theta+} \end{bmatrix} < 0 \tag{33}$$

By the well-known Schur complement lemma [33], we can prove that the inequality (33) is equivalent to

$$\Xi^\top P_{\theta+} \Xi + \begin{bmatrix} (\tau_1 - 1)\, P_\theta & \star & \star \\ S_\theta^{-1} W_\theta H_\theta^{-1} & -2S_\theta^{-1} & \star \\ 0 & 0 & -\tau_2 I \end{bmatrix} < 0 \tag{34}$$

where $\Xi = \begin{bmatrix} A_\theta + B_\theta^u G_\theta H_\theta^{-1} & -B_\theta^u & B_\theta^w \end{bmatrix}$ and $P_{\theta+} = X_{\theta+}^{-1}$. Pre- and post-multiplying (34) by the vector $\begin{bmatrix} x(\kappa)^\top & \Psi(u(\kappa))^\top & w(\kappa)^\top \end{bmatrix}$ and its transpose leads to the following inequality after some simple manipulations:

$$\begin{aligned} \mathbb{V}(x(\kappa+1)) + (\tau_1 - 1)\mathbb{V}(x(\kappa)) - \tau_2 w(\kappa)^\top w(\kappa) \\ - 2\Psi(u)^\top S_\theta^{-1} \left[\Psi(u) - W_\theta H_\theta^{-1} x(\kappa)\right] < 0 \end{aligned} \tag{35}$$

where the positive definite function $\mathbb{V}(x(\kappa))$ is defined as follows:

$$\mathbb{V}(x(\kappa)) = x(\kappa)^\top \sum_{i=1}^{n} \eta_i(\theta) P_i x(\kappa) = x(\kappa)^\top P_\theta x(\kappa) \tag{36}$$

Using Schur complement lemma and the matrix property in (14), it can be deduced from (25) that

$$H_\theta^\top P_\theta H_\theta - \frac{\left(G_{\theta(l)} - W_{\theta(l)}\right)^\top \left(G_{\theta(l)} - W_{\theta(l)}\right)}{u_{\max(l)}^2} \geq 0 \tag{37}$$

Pre- and post- multiplying (37) with $H_\theta^{-\top}$, then it is easily proved that (37) implies $\mathcal{E}_\mathbb{V} \subseteq \mathcal{P}_u$. Since $\mathcal{E}_\mathbb{V} \subseteq \mathcal{P}_u$, by Lemma 1 it follows from (35) that

$$\mathbb{V}(x(\kappa+1)) + (\tau_1 - 1)\mathbb{V}(x(\kappa)) - \tau_2 w(\kappa)^\top w(\kappa) < 0, \quad \forall x \in \mathcal{E}_\mathbb{V} \tag{38}$$

Let us define $\Delta\mathbb{V} = \mathbb{V}(x(\kappa+1)) - \mathbb{V}(x(\kappa))$, the following cases are distinguished.

- If $w = 0$, it can be deduced from (38) that

$$\Delta \mathbb{V} < -\tau_1 \mathbb{V}(x(\kappa)), \quad \forall x \in \mathcal{E}_{\mathbb{V}} \tag{39}$$

which means that all closed-loop trajectories stating from the set $\mathcal{E}_{\mathbb{V}}$ converge asymptotically to the origin with a decay rate less than $\tau_1/2$.

- If $w \neq 0$ and $w \in \mathcal{W}_{\phi}^{\infty}$, the satisfaction of (26) and (38) implies that

$$\Delta \mathbb{V} + \tau_1 \left(\mathbb{V}(x(\kappa)) - 1\right) + \tau_2 \left(\phi - w(\kappa)^\top w(\kappa)\right) < 0, \quad \forall x \in \mathcal{E}_{\mathbb{V}} \tag{40}$$

The condition (40), in turn, guarantees that the set $\mathcal{E}_{\mathbb{V}}$ is robustly positively invariant [34] with respect to the closed-loop system (13). Moreover, it follows from the condition (27) that

$$\begin{bmatrix} P_\theta & C_\theta^\top \\ C_\theta & \gamma I \end{bmatrix} \geq 0 \tag{41}$$

Applying Schur complement lemma to (41), we can prove that

$$z^\top z = x^\top C_\theta^\top C_\theta x \leq \gamma x^\top P_\theta x \leq \gamma, \quad \forall x \in \mathcal{E}_{\mathbb{V}} \tag{42}$$

which means that the $\mathcal{L}_\infty-$norm of the output signal z is bounded: $\|z\|_\infty^2 \leq \gamma$.

The proof of Theorem 1 can be now concluded. □

Remark 1. The design conditions in Theorem 1 are based on the choice of the fuzzy Lyapunov function (36). This type of Lyapunov functions allows reducing effectively the design conservatism compared to the common quadratic Lyapunov function $\mathbb{V}(x(\kappa)) = x(\kappa)^\top P x(\kappa)$. Indeed, the latter is simply a special case of (36) by imposing $P_i = P$, $i \in \Omega_r$. Note that the proposed method can be easily generalized by using more complex fuzzy Lyapunov functions [16] to reduce further the conservatism at the expense of computational cost.

Remark 2. The design conditions presented in Theorem 1 are strictly expressed in terms of linear matrix inequalities which can be effectively solved with available numerical solvers [33]. In this work, the feedback gains G_i, H_i, $i \in \Omega_r$ in (12) are computed with SeDuMi solver and YALMIP toolbox [35].

Remark 3. The decay rate τ_1 in Property 2 is related to the time performance of the closed-loop system [20]. A large value of this tuning parameter leads to a fast convergence time; however the corresponding controller could induce some aggressive closed-loop behaviors. Especially, this situation can get worst if the disturbance signals are directly involved in the system dynamics, for example the lateral wind force and the road curvature in the case of the road-vehicle system (9).

3.4. Comparison Study between Different Control Methods

By means of an academic example, we study here the design conservatism and the numerical complexity of the proposed method compared to the work in [18] dealing with a similar control problem, i.e. constrained T-S fuzzy systems subject to actuator saturation and $\mathcal{L}_\infty$ disturbances.

Example 1. Let us consider the constrained T-S fuzzy system (11) with the following system data [18, 36]:

$$\begin{aligned} A_1 &= \begin{bmatrix} 1 & -\beta \\ -1 & -0.5 \end{bmatrix}, \; B_1^u = \begin{bmatrix} 5+\beta \\ 2\beta \end{bmatrix}, \; B_1^w = \begin{bmatrix} \beta/2 \\ 0 \end{bmatrix}, \; C_1 = \begin{bmatrix} 1 & 0 \end{bmatrix} \\ A_2 &= \begin{bmatrix} 1 & \beta \\ -1 & -0.5 \end{bmatrix}, \; B_2^u = \begin{bmatrix} 5-\beta \\ -2\beta \end{bmatrix}, \; B_2^w = \begin{bmatrix} -\beta/2 \\ 0 \end{bmatrix}, \; C_2 = \begin{bmatrix} 1 & 0 \end{bmatrix} \end{aligned} \tag{43}$$

where $\beta > 0$ and $u_{\max} = 1$. It is also assumed that the T-S fuzzy system (43) is subject to the amplitude-bounded disturbance $w(\kappa) = 0.5\sin(\kappa)$.

Note that the computational complexity of an LMI optimization problem can be estimated as being proportional to $\mathcal{N}_{\text{var}}^3\mathcal{N}_{\text{row}}$, where $\mathcal{N}_{\text{var}}$ is the total number of scalar decision variables and $\mathcal{N}_{\text{row}}$ the total row size of the LMIs. These numbers for two different control methods are given as follows.

- For the design conditions of Theorem 1:

$$\begin{aligned} \mathcal{N}_{\text{row}} &= 2 + rn_u(n_x+1) + r^3(2n_x + n_u + n_w + n_z) \\ \mathcal{N}_{\text{var}} &= 2 + rn_x(n_x+2n_u) + n_x(n_x+1)/2 + n_u(n_u+1)/2 \end{aligned} \tag{44}$$

- For the design conditions of Theorem 2 in [18]:

$$\begin{aligned} \mathcal{N}_{\text{row}} =& r^2(2n_x+n_w)(2+3r(r-1)/2+(r(r-1)/2)^2) \\ &+ 2r(3n_x+n_u+n_w) + r^2(r-1)(3n_x+n_u+n_w)/2 \\ \mathcal{N}_{\text{var}} =& 1 + n_x(n_x+1)/2 + n_u(n_u+1)/2 + rn_x(n_x+n_u) \\ &+ r^2(r^2+(n_x+n_u)^2 + n_x(n_x+1)/2 + (2n_x+n_w)^2) \\ &+ r^4(2n_x+n_w)^2 \end{aligned} \tag{45}$$

Table 2 shows the maximal β, denoted by β^*, for which a stabilizing controller can be designed from two different methods and also the numbers characterizing the complexity of these methods. Observe that the new method provides not only less conservative results but also much lower computational cost. Compared to (44), it can be seen from (45) that the computational complexity of the method in [18] becomes *excessively* important with high dimensional T-S fuzzy systems and/or T-S fuzzy systems with important number of linear subsystems. This represents a major advantage of the proposed control method for real-world applications.

Table 2: Comparison between different design methods

Design conditions	Theorem 1	Theorem 2 in [18]
β^*	1.68	1.55
$\mathcal{N}_{\text{row}}$	56	168
$\mathcal{N}_{\text{var}}$	25	581

4. Automatic Steering Control of Autonomous Vehicle

This section first presents the application of Theorem 1 to the lane keeping control of the autonomous vehicle described in Section 2. Then, simulation results are given to show the effectiveness of the new control method.

4.1. T-S Fuzzy Modeling for Vehicle System

For the control design, let us define the performance output of the vehicle system (9). This variable should represent both lane keeping and driving comfort

$$z = \begin{bmatrix} a_y & \psi_L & y_L \end{bmatrix}^\top \tag{46}$$

Note that the lane keeping performance is represented by the heading error ψ_L and the lateral deviation error y_L. The driving comfort is represented by the lateral acceleration $a_y \cong v_x r$. Note also that all components of z can be expressed by those of the state x in (9) as follows:

$$z = \mathbf{C}x = \begin{bmatrix} 0 & v_x & 0 & 0 \\ 0 & 0 & 1 & 0 \\ 0 & 0 & 0 & 1 \end{bmatrix} x \tag{47}$$

We note also that the matrices $\mathbf{A}$, $\mathbf{B}_w$ in (9)-(10) and $\mathbf{C}$ in (47) depend *nonlinearly* on the vehicle speed which is measured and bounded

$$v_x, \quad 1/v_x, \quad 1/v_x^2, \quad v_{\min} \leq v_x \leq v_{\max} \tag{48}$$

where $v_{\min} = 8$ [m/s] and $v_{\max} = 30$ [m/s]. Hence, a natural choice of premise variables to derive the T-S fuzzy representation (11) of vehicle model $\mathbf{\Sigma}_v$ would be $\theta_* = \begin{bmatrix} v_x & 1/v_x & 1/v_x^2 \end{bmatrix}^\top \in \mathbb{R}^3$. Using the sector nonlinearity approach [20], this choice leads to an exact T-S fuzzy model of (9) with $2^3 = 8$ linear subsystems. However, this vehicle T-S model would be too *expensive* in terms of numerical computation for control design, and especially for real-time implementation. In this work, we make use of the well-known Taylor's approximation (first order)

to exploit the strong relationship between v_x, $1/v_x$ and $1/v_x^2$. Therefore, the numerical complexity of the proposed control method can be significantly reduced. Concretely, one has

$$\begin{aligned} &\frac{1}{v_x} = \frac{1}{v_0} + \frac{1}{v_1}\Delta_x, \quad v_x \cong v_0\left(1 - \frac{v_0}{v_1}\Delta_x\right), \quad \frac{1}{v_x^2} \cong \frac{1}{v_0^2}\left(1 + 2\frac{v_0}{v_1}\Delta_x\right) \\ &\Delta_{\min} \leq \Delta_x \leq \Delta_{\max}, \quad \Delta_{\min} = -1, \quad \Delta_{\max} = 1 \end{aligned} \tag{49}$$

where the measured parameter Δ_x is used to describe the variation of v_x between its lower and upper bounds. The two constants v_0 and v_1 in (49) are given by

$$v_0 = \frac{2v_{\min}v_{\max}}{v_{\min} + v_{\max}}, \quad v_1 = \frac{2v_{\min}v_{\max}}{v_{\min} - v_{\max}}.$$

Replacing (49) into (9), we obtain a vehicle model $\mathbf{\Sigma}_v(\Delta_x)$ where the matrices $\mathbf{A}$ and $\mathbf{B}_w$ in (10) depend now *exclusively* on the time-varying parameter Δ_x. Choosing $\theta = \Delta_x \in \mathbb{R}$ as new premise variable and using the sector nonlinearity approach, the T-S fuzzy model (11) of this vehicle model has only 2 linear subsystems whose matrices are given by

$$\begin{aligned} \mathbf{\Sigma}_{v1}: &\ \mathbf{A}(\Delta_{\min}), \ \mathbf{B}_u(\Delta_{\min}), \ \mathbf{B}_w(\Delta_{\min}) \\ \mathbf{\Sigma}_{v2}: &\ \mathbf{A}(\Delta_{\max}), \ \mathbf{B}_u(\Delta_{\max}), \ \mathbf{B}_w(\Delta_{\max}) \end{aligned} \tag{50}$$

where the expressions of $\mathbf{A}$, $\mathbf{B}_u$ and $\mathbf{B}_w$ are given in (10). The two corresponding membership functions of this T-S fuzzy model are defined as follows:

$$\eta_1(\Delta_x) = \frac{1 - \Delta_x}{2}, \quad \eta_2(\Delta_x) = 1 - \eta_1(\Delta_x).$$

As stated in Section 1, the actuator saturation of the steering system should be *explicitly* taken into account in the design procedure to prevent the loss of closed-loop stability during some specific driving scenarios. Here, the constraint on the control input is $u_{\max} = 10$ [deg]. This input constraint is the limitation of the steering angle imposed to the studied autonomous vehicle. We can now design the vehicle steering control actions by solving the LMI conditions of Theorem 1.

Some obtained numerical results are given as follows:

$$G_1 = \begin{bmatrix} -0.025 & -0.387 & -0.027 & -0.080 \end{bmatrix},$$
$$G_2 = \begin{bmatrix} -0.023 & -0.491 & -0.022 & -0.054 \end{bmatrix},$$
$$H_1 = \begin{bmatrix} 0.082 & -0.114 & -0.030 & -0.143 \\ -0.089 & 2.608 & -0.137 & -0.488 \\ -0.031 & -0.129 & 0.052 & 0.120 \\ -0.144 & -0.438 & 0.119 & 0.495 \end{bmatrix},$$
$$H_2 = \begin{bmatrix} 0.067 & -0.035 & -0.029 & -0.135 \\ -0.039 & 1.614 & -0.107 & -0.386 \\ -0.029 & -0.108 & 0.051 & 0.113 \\ -0.139 & -0.392 & 0.113 & 0.489 \end{bmatrix},$$

and the corresponding Lyapunov matrices are

$$P_1 = \begin{bmatrix} 79.729 & 8.922 & -5.911 & 32.048 \\ 8.922 & 1.639 & -0.116 & 3.991 \\ -5.911 & -0.116 & 43.217 & -12.299 \\ 32.048 & 3.991 & -12.299 & 17.757 \end{bmatrix},$$
$$P_2 = \begin{bmatrix} 92.599 & 10.740 & -3.234 & 35.347 \\ 10.740 & 2.032 & 0.165 & 4.587 \\ -3.234 & 0.165 & 42.078 & -10.911 \\ 35.347 & 4.587 & -10.911 & 18.360 \end{bmatrix}.$$

Note that two Lyapunov matrices are significantly different which justifies *a posteriori* the interest of the non-quadratic Lyapunov function (36) for the proposed T-S fuzzy control method.

4.2. Simulation Results

For the following numerical simulations, the designed non-PDC controller is tested with the road-vehicle model presented in Section 2.

4.2.1. Scenario 1: Control input saturation

We assume that the vehicle system is not *well initialized* where its initial state $x_0^\top = \begin{bmatrix} 0 & 0 & 0.25 & 0.5 \end{bmatrix}$ does not correspond to the system origin, i.e. the lane centreline. The vehicle responses in this case are indicated in Figure 2. It can be clearly observed that despite an important level of actuator saturation at the beginning of the simulation, all vehicle state variables converge to the origin.

Note that the non-PDC controller proposed in [36] cannot provide a stable closed-loop behaviors for the studied autonomous vehicle under the same simulation conditions as shown in Figure 3. Indeed, since the input constraint was not

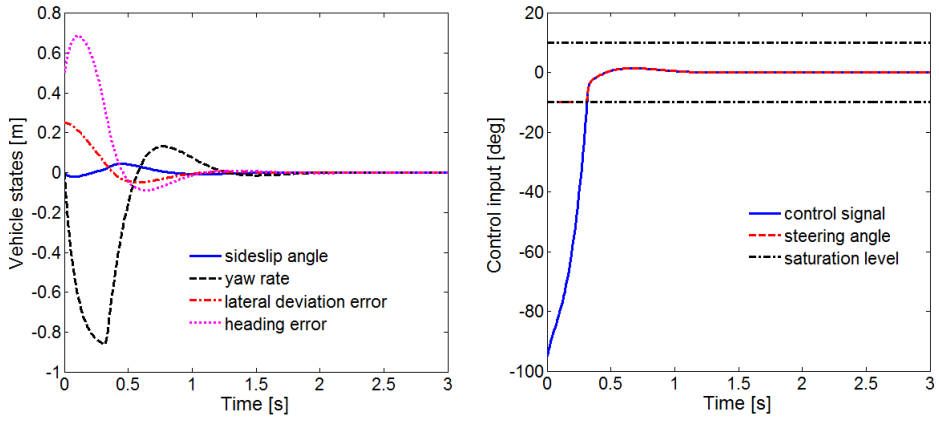

Figure 2: Vehicle responses in the presence of actuator saturation with the proposed method.

explicitly considered in the control procedure with the design conditions in [36], therefore the obtained fuzzy controller cannot provide any guarantee on the stability of the vehicle in case of important actuator saturation. For the following driving

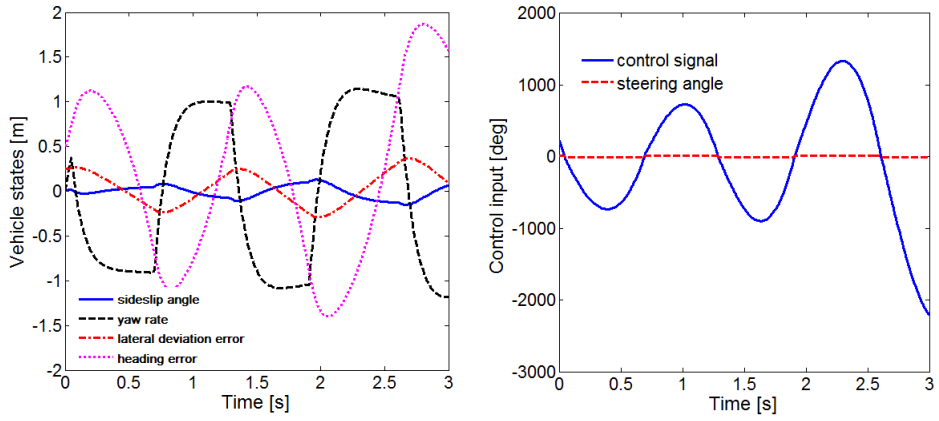

Figure 3: Vehicle responses obtained with the control method in [36] for the test in Scenario 1.

test scenarios, the vehicle will be initialized at the lane centreline.

4.2.2. Scenario 2: Lane keeping performance

This scenario aims to show the lane-keeping performance of the proposed controller in the case where the road is composed by several sections with different

levels of curvature. To this end, we use the digital database of the Satory test track near Paris, France [37] for simulation purposes, see Figure 4 (left). The corresponding road curvature and vehicle speed are respectively depicted in Figure 4 (right). As can be observed, the vehicle speed for this test strongly varies within its range $v_x \in [8, 30]$. This clearly justifies the interest of the proposed T-S fuzzy model-based control method.

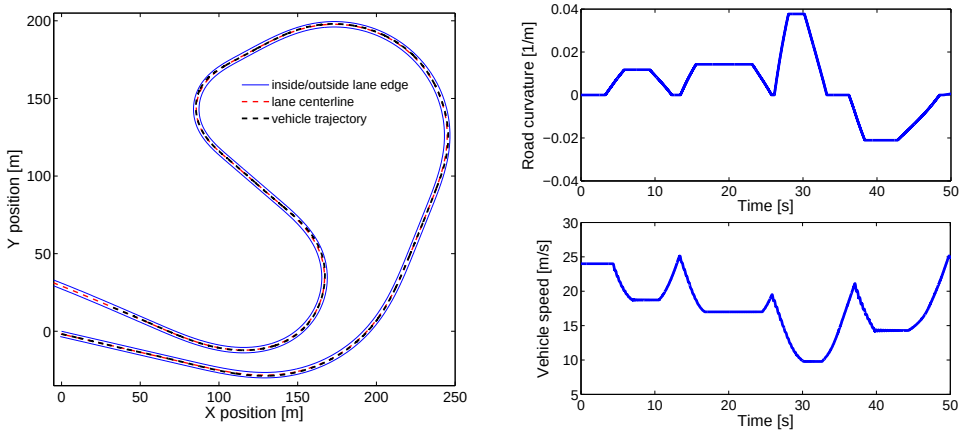

Figure 4: Vehicle trajectory performed by the automatic lane-keeping controller (left). Digital database corresponding to the test track of Scenario 2 (right).

Observe in Figure 4 (left) that the proposed T-S fuzzy controller is able to guarantee a good lane keeping performance for the studied autonomous vehicle. This is also confirmed by the fact that the variables representing lane keeping errors are relatively small and strictly remain within their practical domain of variation during the whole simulation test as indicated in Figure 5.

5. Experimental Results

To further examine the practical performance of the designed controller, a series of experiments are implemented on the advanced SHERPA dynamic simulator, see Figure 6. This simulator is in the form of a Peugeot 206 vehicle fixed on a Stewart platform, the whole is positioned in front of five flat panel displays providing a visual field of 240°. Based on a distributed computing architecture, this complex simulator is structured around a SCANeR network connecting fifteen PC-type workstations. The whole software of the SHERPA simulator is developed

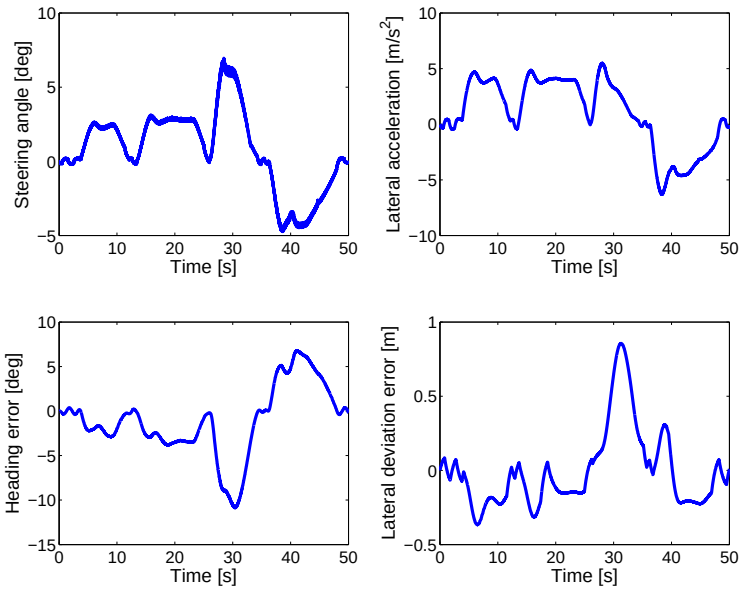

Figure 5: Simulation results of Scenario 2: steering control actions and vehicle responses.

with RTMaps environment composed by several modules which are in charge of different tasks: perception, planning, human-machine interface.

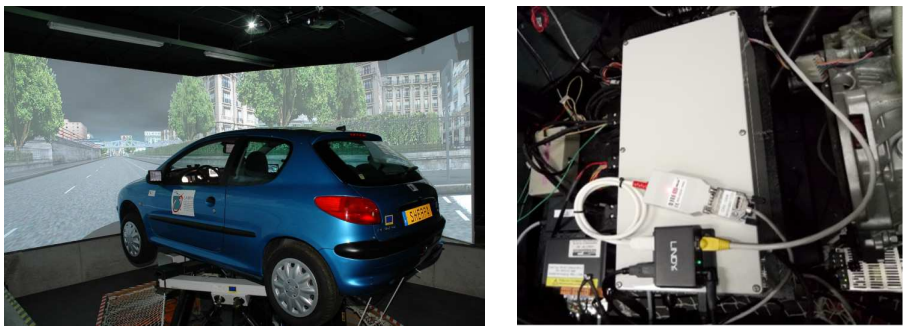

Figure 6: SHERPA interactive dynamic driving simulator (left). Data acquisition system (right).

5.1. Scenario 3: Rejection of wind disturbance

For this scenario, the vehicle speed is fixed at $v_x = 15$ [m/s] and the vehicle dynamics is affected by an important lateral wind force for a duration of $5s$ as shown in Figure 7. The vehicle variables are therefore perturbed. However, the proposed T-S fuzzy controller is able to reject effectively the disturbance effect and all states converge to the origin at the end of the test scenario. Moreover, we can see also from Figure 7 that state variables representing the vehicle performance, namely sideslip angle β, vehicle yaw rate r, heading error ψ_L, and lateral deviation error y_L are very small under the effect of the strong wind force. This also illustrates the performance of the proposed controller.

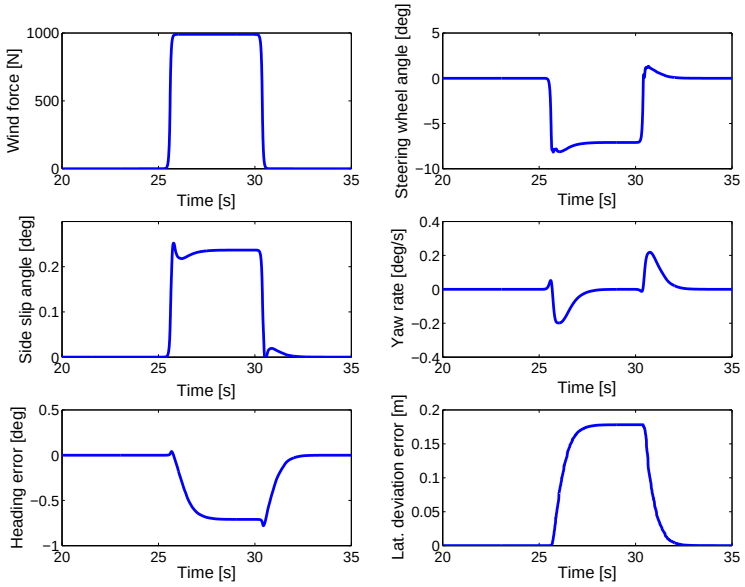

Figure 7: Control performance in terms of lateral wind force attenuation.

5.2. Scenario 4: Vehicle stability performance with ISO chicane test

The normalized chicane test is widely employed to verify the stability performance of autonomous vehicles in an extreme driving situation. This corresponds to an obstacle avoidance scenario as indicated in Figure 8. For this experiment, the vehicle speed is fixed as $v_x = 10$ [m/s]. The lateral trajectory performed with the proposed non-PDC controller and the steering control signal corresponds to this scenario are respectively shown in Figures 9 (a) and (d). As indicated in Figures 9 (b), (c), (e) and (f), the studied autonomous vehicle is perfectly able to perform the

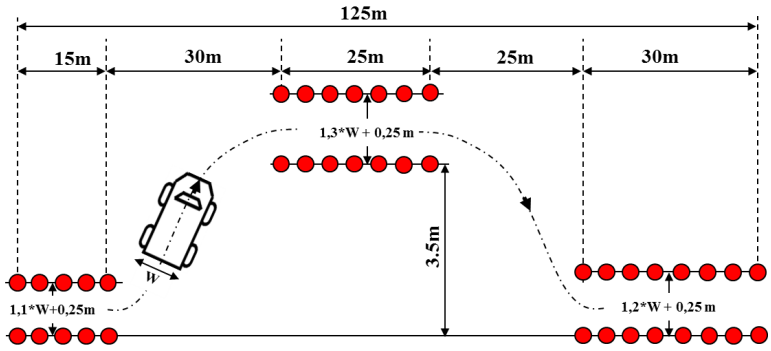

Figure 8: ISO chicane test for vehicle stability evaluation.

chicane test with the designed controller since all variables representing the lane following performance of the vehicle are relatively small during the whole test, i.e. the autonomous vehicle always remains inside the predefined lane.

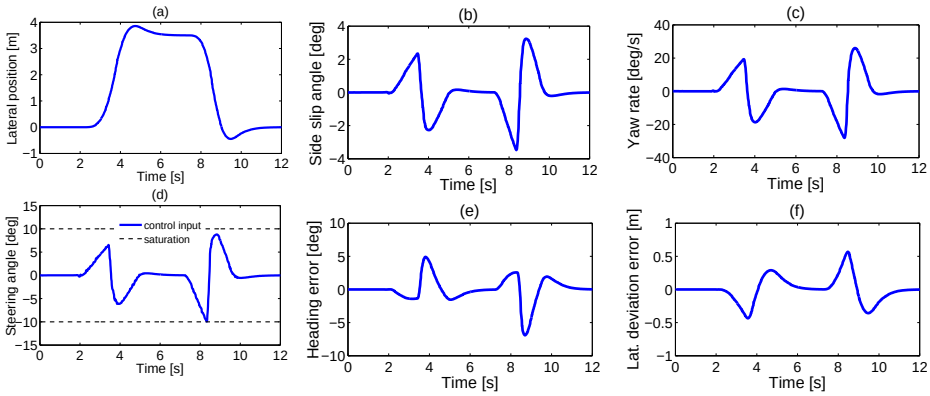

Figure 9: Lateral trajectory performed with the proposed non-PDC controller (a); steering control angle (d); response of the autonomous vehicle (b), (c), (e) and (f).

5.3. Scenario 5: Lane keeping with the complete Satory test track

This experiment aims to show the lane keeping performance of the proposed T-S fuzzy controller during the whole Satory test track, see Figure 10 (a). Figures 10 (b), (c), and (d) show respectively the road curvature of Satory test track, the vehicle speed for this test, and the designed steering control signal. Despite a large variation of vehicle speed, it can be observed from the vehicle variables representing the lane keeping performance in Figure 11 that the proposed non-PDC

controller guarantees a good control performance for the whole test with small lane keeping errors. In particular, for the first four curves although the vehicle speed is different between Scenarios 2 and 5, the vehicle responses (steering angle and vehicle variables) obtained for both cases are rather similar. This fact demonstrates not only the advantage of considering the speed variation into the control design procedure but also the strong usefulness of numerical simulations.

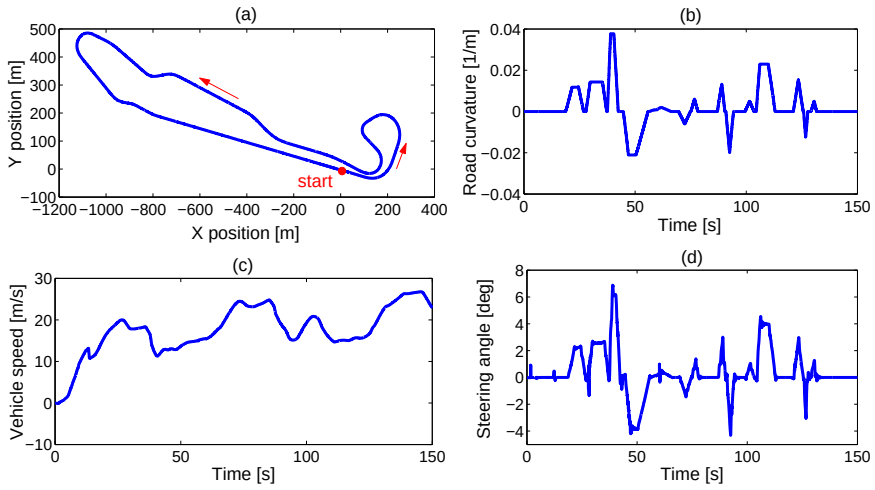

Figure 10: Satory track and lane keeping test condition.

6. Concluding Remarks

A new LMI-based control method for the automatic lane keeping of autonomous vehicles subject to actuator saturation has been proposed. The vehicle system is approximated by means of T-S fuzzy modeling to deal with a large variation range of vehicle speed. This method relies on the use of a fuzzy Lyapunov function to reduce the conservatism of the results. Moreover, two specific realizations have been proposed to ease the real-time control implementation: (1) Taylor's approximation method is used to reduce the model complexity, (2) the control design of an input-saturated non-PDC controller has been directly synthesized in discrete-time domain. Extensive validation with both numerical simulations and experimental tests has been carried out to verify the practical performance of the proposed control method. Future works focus on exploiting the proposed design method for the control issues of semi-autonomous vehicles. To this end, the human driver behaviors should be integrated into the control design procedure [37].

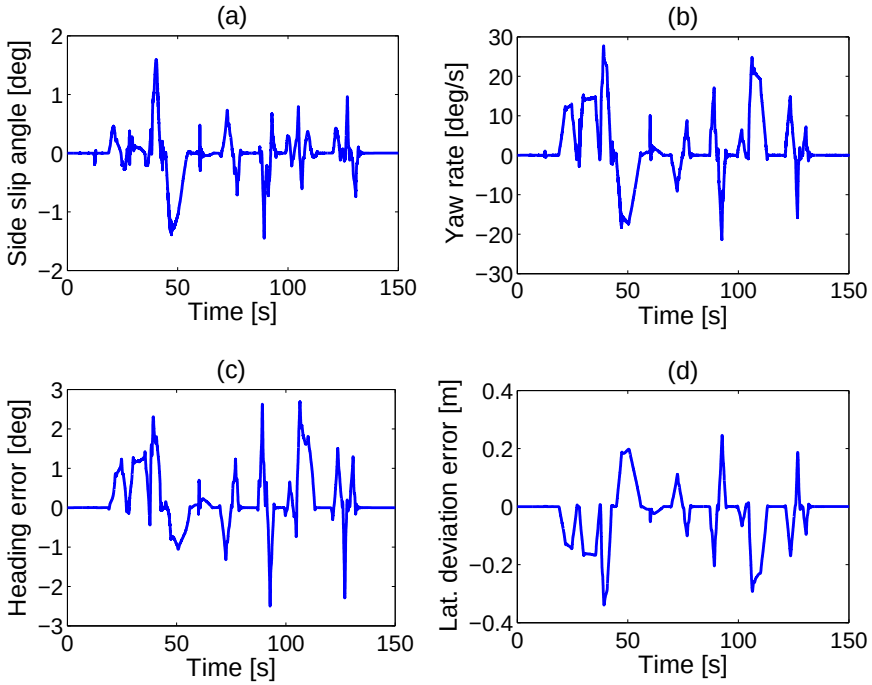

Figure 11: Automatic lane keeping performance during the whole Satory test track.

Acknowledgement

This work has been done in the framework of the CoCoVeA research program (ANR-13-TDMO-0005), funded by the National Research Agency. This work was also sponsored by the International Campus on Safety and Intermodality in Transportation, the Nord-Pas-de-Calais Region, the European Community, the Regional Delegation for Research and Technology, the Ministry of Higher Education and Research, and the French National Center for Scientific Research.

References

[1] L. D. Baskar, B. De Schutter, J. Hellendoorn, Z. Papp, Traffic control and intelligent vehicle highway systems: A survey, IET Intell. Transp. Syst. 5 (1) (2011) 38–52.

[2] R. Rajamani, Vehicle Dynamics and Control, Boston: Springer US, 2012.

[3] X. Li, Z. Sun, D. Cao, D. Liu, H. He, Development of a new integrated local

trajectory planning and tracking control framework for autonomous ground vehicles, Mech. Syst. Signal Process. 87 (2017) 118–137.

[4] L. Li, Y. Lu, R. Wang, J. Chen, A three-dimensional dynamics control framework of vehicle lateral stability and rollover prevention via active braking with mpc, IEEE Trans. Ind. Electron. 64 (4) (2017) 3389–3401.

[5] H. Zhang, J. Wang, Vehicle lateral dynamics control through AFS/DYC and robust gain-scheduling approach, IEEE Trans. Veh. Technol. 65 (1) (2016) 489–494.

[6] R. Bishop, Intelligent vehicle applications worldwide, IEEE Intell. Syst. Appl. 15 (1) (2000) 78–81.

[7] A.-T. Nguyen, C. Sentouh, J.-C. Popieul, Driver-automation cooperative approach for shared steering control under multiple system constraints: Design and experiments, IEEE Trans. Ind. Electron. 64 (5) (2017) 3819–3830.

[8] J. Wang, G. Zhang, R. Wang, S. C. Schnelle, J. Wang, A gain-scheduling driver assistance trajectory-following algorithm considering different driver steering characteristics, IEEE Trans. Intell. Transp. Syst. 18 (5) (2017) 1097–1108.

[9] J. Wang, M. Dai, G. Yin, N. Chen, Output-feedback robust control for vehicle path tracking considering different human drivers' characteristics, Mechatronics, 2017. doi:http://dx.doi.org/10.1016/j.mechatronics.2017.05.001.

[10] N. Enache, S. Mammar, M. Netto, B. Lusetti, Driver steering assistance for lane-departure avoidance based on hybrid automata and composite Lyapunov function, IEEE Trans. Intell. Transp. Syst. 11 (1) (2010) 28–39.

[11] G. Tagne, R. Talj, A. Charara, Design and comparison of robust nonlinear controllers for the lateral dynamics of intelligent vehicles, IEEE Trans. Intell. Transp. Syst. 17 (3) (2016) 796–809.

[12] J. Naranjo, C. Gonzalez, R. Garcia, T. de Pedro, R. Haber, Power-steering control architecture for automatic driving, IEEE Trans. Intell. Transp. Syst. 6 (4) (2005) 406–415.

[13] V. Cerone, M. Milanese, D. Regruto, Combined automatic lane-keeping and driver's steering through a 2-DOF control strategy, IEEE Trans. Control Syst. Technol. 17 (1) (2009) 135–142.

[14] R. Marino, S. Scalzi, M. Netto, Nested PID steering control for lane keeping in autonomous vehicles, Control Eng. Pract. 19 (12) (2011) 1459–1467.

[15] M. A. Sotelo, F. J. Rodriguez, L. Magdalena, Virtuous: Vision-based road transportation for unmanned operation on urban-like scenarios, IEEE Trans. Intell. Transp. Syst. 5 (2) (2004) 69–83.

[16] A.-T. Nguyen, K. Tanaka, A. Dequidt, M. Dambrine, Static output feedback design for a class of constrained Takagi-Sugeno fuzzy systems, J. Franklin. Inst. 354 (7) (2017) 2856–2870.

[17] A.-T. Nguyen, A. Dequidt, M. Dambrine, Anti-windup based dynamic output feedback controller design with performance consideration for constrained Takagi-Sugeno systems, Eng. Appl. Artif. Intell. 40 (2015) 76–83.

[18] T. Zou, S. Li, Stabilization via extended nonquadratic boundedness for constrained nonlinear systems in Takagi-Sugeno's form, J. Franklin. Inst. 348 (10) (2011) 2849–2862.

[19] T. Takagi, M. Sugeno, Fuzzy identification of systems and its applications to modeling and control, IEEE Trans. Syst. Man, Cybern. B, Cybern. SMC-15 (1) (1985) 116–132.

[20] K. Tanaka, H. O. Wang, Fuzzy Control Systems Design and Analysis: A Linear Matrix Inequality Approach, John Wiley & Sons, 2004.

[21] S. Xu, G. Sun, W. Sun, Fuzzy logic based fault-tolerant attitude control for nonlinear flexible spacecraft with sampled-data input, J. Franklin. Inst. 354 (5) (2017) 2125–2156.

[22] M. S. Sadeghi, N. Vafamand, M. H. Khooban, LMI-based stability analysis and robust controller design for a class of nonlinear chaotic power systems, J. Franklin. Inst. 353 (13) (2016) 2835–2858.

[23] A. Sala, C. Ariño, Asymptotically necessary and sufficient conditions for stability and performance in fuzzy control: Applications of Polya's theorem, Fuzzy Sets and Syst. 158 (24) (2007) 2671–2686.

[24] H. Du, N. Zhang, Fuzzy control for nonlinear uncertain electrohydraulic active suspensions with input constraint, IEEE Trans. Fuzzy Syst. 17 (2) (2009) 343–356.

[25] H. Dahmani, O. Pagès, A. El Hajjaji, Observer-based state feedback control for vehicle chassis stability in critical situations, IEEE Trans. Control Syst. Technol. 24 (2) (2016) 636–643.

[26] A.-T. Nguyen, M. Dambrine, J. Lauber, Lyapunov-based robust control design for a class of switching non-linear systems subject to input saturation: application to engine control, IET Control Theory Appl. 8 (2014) 1789–1802.

[27] S.-H. Kim, C. Lee, J. Park, $\mathcal{H}_\infty$ state-feedback control for fuzzy systems with input saturation via fuzzy weighting-dependent Lyapunov functions, Comput. Math. Appl. 57 (6) (2009) 981–990.

[28] D. Saifia, M. Chadli, H. Karimi, S. Labiod, Fuzzy control for electric power steering system with assist motor current input constraints, J. Franklin. Inst. 352 (2) (2015) 562–576.

[29] A.-T. Nguyen, R. Márquez, A. Dequidt, An augmented system approach for LMI-based control design of constrained Takagi-Sugeno fuzzy systems, Eng. Appl. Artif. Intell. 61 (2017) 96 – 102.

[30] A. Benzaouia, F. Mesquine, M. Benhayoun, H. Schulte, S. Georg, Stabilization of positive constrained T-S fuzzy systems: Application to a Buck converter, J. Franklin. Inst. 351 (8) (2014) 4111–4123.

[31] H. Pacejka, Tire and Vehicle Dynamics, Elsevier, 2005.

[32] H. Tuan, P. Apkarian, T. Narikiyo, Y. Yamamoto, Parameterized linear matrix inequality techniques in fuzzy control system design, IEEE Trans. Fuzzy Syst. 9 (2) (2001) 324–332.

[33] S. Boyd, L. El Ghaoui, E. Feron, V. Balakrishnan, Linear Matrix Inequalities in System and Control Theory, Vol. 15, SIAM, Philadelphia, 1994.

[34] S. Tarbouriech, G. Garcia, J. Gomes da Silva Jr., I. Queinnec, Stability and Stabilization of Linear Systems with Saturating Actuators, London: Springer-Verlag, 2011.

[35] J. Löfberg, YALMIP: A toolbox for modeling and optimization in MATLAB, in: IEEE Int. Symp. Comput. Aided Control Syst. Des., Taipei, 2004, pp. 284–289.

[36] T.-M. Guerra, L. Vermeiren, LMI-based relaxed non-quadratic stabilization conditions for nonlinear systems in the Takagi-Sugeno's form, Automatica 40 (5) (2004) 823–829.

[37] A.-T. Nguyen, C. Sentouh, J. C. Popieul, Sensor reduction for driver-automation shared steering control via an adaptive authority allocation strategy, IEEE/ASME Trans. Mechatron., 2017. doi:10.1109/TMECH.2017.2698216.